FERMILAB-PUB-04/297-E

A Measurement of the Ratio of Inclusive Cross Sections $\sigma(p\bar{p} \to Z + b \text{ jet})/\sigma(p\bar{p} \to Z + \text{jet})$ at $\sqrt{s} = 1.96$ TeV

V.M. Abazov,[33] B. Abbott,[70] M. Abolins,[61] B.S. Acharya,[27] M. Adams,[48] T. Adams,[46] M. Agelou,[17] J.-L. Agram,[18] S.H. Ahn,[29] M. Ahsan,[55] G.D. Alexeev,[33] G. Alkhazov,[37] A. Alton,[60] G. Alverson,[59] G.A. Alves,[2] M. Anastasoaie,[32] S. Anderson,[42] B. Andrieu,[16] Y. Arnoud,[13] A. Askew,[74] B. Åsman,[38] O. Atramentov,[53] C. Autermann,[20] C. Avila,[7] F. Badaud,[12] A. Baden,[57] B. Baldin,[47] P.W. Balm,[31] S. Banerjee,[27] E. Barberis,[59] P. Bargassa,[74] P. Baringer,[54] C. Barnes,[40] J. Barreto,[2] J.F. Bartlett,[47] U. Bassler,[16] D. Bauer,[51] A. Bean,[54] S. Beauceron,[16] M. Begel,[66] A. Bellavance,[63] S.B. Beri,[26] G. Bernardi,[16] R. Bernhard,[47,*] I. Bertram,[39] M. Besançon,[17] R. Beuselinck,[40] V.A. Bezzubov,[36] P.C. Bhat,[47] V. Bhatnagar,[26] M. Binder,[24] K.M. Black,[58] I. Blackler,[40] G. Blazey,[49] F. Blekman,[31] S. Blessing,[46] D. Bloch,[18] U. Blumenschein,[22] A. Boehnlein,[47] O. Boeriu,[52] T.A. Bolton,[55] F. Borcherding,[47] G. Borissov,[39] K. Bos,[31] T. Bose,[65] A. Brandt,[72] R. Brock,[61] G. Brooijmans,[65] A. Bross,[47] N.J. Buchanan,[46] D. Buchholz,[50] M. Buehler,[48] V. Buescher,[22] S. Burdin,[47] T.H. Burnett,[76] E. Busato,[16] J.M. Butler,[58] J. Bystricky,[17] W. Carvalho,[3] B.C.K. Casey,[71] N.M. Cason,[52] H. Castilla-Valdez,[30] S. Chakrabarti,[27] D. Chakraborty,[49] K.M. Chan,[66] A. Chandra,[27] D. Chapin,[71] F. Charles,[18] E. Cheu,[42] L. Chevalier,[17] D.K. Cho,[66] S. Choi,[45] T. Christiansen,[24] L. Christofek,[54] D. Claes,[63] B. Clément,[18] C. Clément,[38] Y. Coadou,[5] M. Cooke,[74] W.E. Cooper,[47] D. Coppage,[54] M. Corcoran,[74] J. Coss,[19] A. Cothenet,[14] M.-C. Cousinou,[14] S. Crépé-Renaudin,[13] M. Cristetiu,[45] M.A.C. Cummings,[49] D. Cutts,[71] H. da Motta,[2] B. Davies,[39] G. Davies,[40] G.A. Davis,[50] K. De,[72] P. de Jong,[31] S.J. de Jong,[32] E. De La Cruz-Burelo,[30] C. De Oliveira Martins,[3] S. Dean,[41] F. Déliot,[17] P.A. Delsart,[19] M. Demarteau,[47] R. Demina,[66] P. Demine,[17] D. Denisov,[47] S.P. Denisov,[36] S. Desai,[67] H.T. Diehl,[47] M. Diesburg,[47] M. Doidge,[39] H. Dong,[67] S. Doulas,[59] L. Duflot,[15] S.R. Dugad,[27] A. Duperrin,[14] J. Dyer,[61] A. Dyshkant,[49] M. Eads,[49] D. Edmunds,[61] T. Edwards,[41] J. Ellison,[45] J. Elmsheuser,[24] J.T. Eltzroth,[72] V.D. Elvira,[47] S. Eno,[57] P. Ermolov,[35] O.V. Eroshin,[36] J. Estrada,[47] D. Evans,[40] H. Evans,[65] A. Evdokimov,[34] V.N. Evdokimov,[36] J. Fast,[47] S.N. Fatakia,[58] L. Feligioni,[58] T. Ferbel,[66] F. Fiedler,[24] F. Filthaut,[32] W. Fisher,[64] H.E. Fisk,[47] M. Fortner,[49] H. Fox,[22] W. Freeman,[47] S. Fu,[47] S. Fuess,[47] T. Gadfort,[76] C.F. Galea,[32] E. Gallas,[47] E. Galyaev,[52] C. Garcia,[66] A. Garcia-Bellido,[76] J. Gardner,[54] V. Gavrilov,[34] P. Gay,[12] D. Gelé,[18] R. Gelhaus,[45] K. Genser,[47] C.E. Gerber,[48] Y. Gershtein,[71] G. Ginther,[66] T. Golling,[21] B. Gómez,[7] K. Gounder,[47] A. Goussiou,[52] P.D. Grannis,[67] S. Greder,[18] H. Greenlee,[47] Z.D. Greenwood,[56] E.M. Gregores,[4] Ph. Gris,[12] J.-F. Grivaz,[15] L. Groer,[65] S. Grünendahl,[47] M.W. Grünewald,[28] S.N. Gurzhiev,[36] G. Gutierrez,[47] P. Gutierrez,[70] A. Haas,[65] N.J. Hadley,[57] S. Hagopian,[46] I. Hall,[70] R.E. Hall,[44] C. Han,[60] L. Han,[41] K. Hanagaki,[47] K. Harder,[55] R. Harrington,[59] J.M. Hauptman,[53] R. Hauser,[61] J. Hays,[50] T. Hebbeker,[20] D. Hedin,[49] J.M. Heinmiller,[48] A.P. Heinson,[45] U. Heintz,[58] C. Hensel,[54] G. Hesketh,[59] M.D. Hildreth,[52] R. Hirosky,[75] J.D. Hobbs,[67] B. Hoeneisen,[11] M. Hohlfeld,[23] S.J. Hong,[29] R. Hooper,[71] P. Houben,[31] Y. Hu,[67] J. Huang,[51] I. Iashvili,[45] R. Illingworth,[47] A.S. Ito,[47] S. Jabeen,[54] M. Jaffré,[15] S. Jain,[70] V. Jain,[68] K. Jakobs,[22] A. Jenkins,[40] R. Jesik,[40] K. Johns,[42] M. Johnson,[47] A. Jonckheere,[47] P. Jonsson,[40] H. Jöstlein,[47] A. Juste,[47] M.M. Kado,[43] D. Käfer,[20] W. Kahl,[55] S. Kahn,[68] E. Kajfasz,[14] A.M. Kalinin,[33] J. Kalk,[61] D. Karmanov,[35] J. Kasper,[58] D. Kau,[46] R. Kehoe,[73] S. Kermiche,[14] S. Kesisoglou,[71] A. Khanov,[66] A. Kharchilava,[52] Y.M. Kharzheev,[33] K.H. Kim,[29] B. Klima,[47] M. Klute,[21] J.M. Kohli,[26] M. Kopal,[70] V.M. Korablev,[36] J. Kotcher,[68] B. Kothari,[65] A. Koubarovsky,[35] A.V. Kozelov,[36] J. Kozminski,[61] S. Krzywdzinski,[47] S. Kuleshov,[34] Y. Kulik,[47] S. Kunori,[57] A. Kupco,[17] T. Kurča,[19] S. Lager,[38] N. Lahrichi,[17] G. Landsberg,[71] J. Lazoflores,[46] A.-C. Le Bihan,[18] P. Lebrun,[19] S.W. Lee,[29] W.M. Lee,[46] A. Leflat,[35] F. Lehner,[47,*] C. Leonidopoulos,[65] P. Lewis,[40] J. Li,[72] Q.Z. Li,[47] J.G.R. Lima,[49] D. Lincoln,[47] S.L. Linn,[46] J. Linnemann,[61] V.V. Lipaev,[36] R. Lipton,[47] L. Lobo,[40] A. Lobodenko,[37] M. Lokajicek,[10] A. Lounis,[18] H.J. Lubatti,[76] L. Lueking,[47] M. Lynker,[52] A.L. Lyon,[47] A.K.A. Maciel,[49] R.J. Madaras,[43] P. Mättig,[25] A. Magerkurth,[60] A.-M. Magnan,[13] N. Makovec,[15] P.K. Mal,[27] S. Malik,[56] V.L. Malyshev,[33] H.S. Mao,[6] Y. Maravin,[47] M. Martens,[47] S.E.K. Mattingly,[71] A.A. Mayorov,[36] R. McCarthy,[67] R. McCroskey,[42] D. Meder,[23] H.L. Melanson,[47] A. Melnitchouk,[62] M. Merkin,[35] K.W. Merritt,[47] A. Meyer,[20] H. Miettinen,[74] D. Mihalcea,[49] J. Mitrevski,[65] N. Mokhov,[47] J. Molina,[3] N.K. Mondal,[27] H.E. Montgomery,[47] R.W. Moore,[5] G.S. Muanza,[19] M. Mulders,[47] Y.D. Mutaf,[67] E. Nagy,[14] M. Narain,[58] N.A. Naumann,[32] H.A. Neal,[60] J.P. Negret,[7] S. Nelson,[46] P. Neustroev,[37] C. Noeding,[22] A. Nomerotski,[47] S.F. Novaes,[4] T. Nunnemann,[24] E. Nurse,[41] V. O'Dell,[47] D.C. O'Neil,[5] V. Oguri,[3] N. Oliveira,[3] N. Oshima,[47] G.J. Otero y Garzón,[48] P. Padley,[74] N. Parashar,[56] J. Park,[29]

S.K. Park,[29] J. Parsons,[65] R. Partridge,[71] N. Parua,[67] A. Patwa,[68] P.M. Perea,[45] E. Perez,[17] O. Peters,[31] P. Pétroff,[15] M. Petteni,[40] L. Phaf,[31] R. Piegaia,[1] P.L.M. Podesta-Lerma,[30] V.M. Podstavkov,[47] Y. Pogorelov,[52] B.G. Pope,[61] W.L. Prado da Silva,[3] H.B. Prosper,[46] S. Protopopescu,[68] M.B. Przybycien,[50,†] J. Qian,[60] A. Quadt,[21] B. Quinn,[62] K.J. Rani,[27] P.A. Rapidis,[47] P.N. Ratoff,[39] N.W. Reay,[55] S. Reucroft,[59] M. Rijssenbeek,[67] I. Ripp-Baudot,[18] F. Rizatdinova,[55] C. Royon,[17] P. Rubinov,[47] R. Ruchti,[52] G. Sajot,[13] A. Sánchez-Hernández,[30] M.P. Sanders,[41] A. Santoro,[3] G. Savage,[47] L. Sawyer,[56] T. Scanlon,[40] R.D. Schamberger,[67] H. Schellman,[50] P. Schieferdecker,[24] C. Schmitt,[25] A.A. Schukin,[36] A. Schwartzman,[64] R. Schwienhorst,[61] S. Sengupta,[46] H. Severini,[70] E. Shabalina,[48] M. Shamim,[55] V. Shary,[17] W.D. Shephard,[52] D. Shpakov,[59] R.A. Sidwell,[55] V. Simak,[9] V. Sirotenko,[47] P. Skubic,[70] P. Slattery,[66] R.P. Smith,[47] K. Smolek,[9] G.R. Snow,[63] J. Snow,[69] S. Snyder,[68] S. Söldner-Rembold,[41] X. Song,[49] Y. Song,[72] L. Sonnenschein,[58] A. Sopczak,[39] M. Sosebee,[72] K. Soustruznik,[8] M. Souza,[2] B. Spurlock,[72] N.R. Stanton,[55] J. Stark,[13] J. Steele,[56] G. Steinbrück,[65] K. Stevenson,[51] V. Stolin,[34] A. Stone,[48] D.A. Stoyanova,[36] J. Strandberg,[38] M.A. Strang,[72] M. Strauss,[70] R. Ströhmer,[24] M. Strovink,[43] L. Stutte,[47] S. Sumowidagdo,[46] A. Sznajder,[3] M. Talby,[14] P. Tamburello,[42] W. Taylor,[5] P. Telford,[41] J. Temple,[42] S. Tentindo-Repond,[46] E. Thomas,[14] B. Thooris,[17] M. Tomoto,[47] T. Toole,[57] J. Torborg,[52] S. Towers,[67] T. Trefzger,[23] S. Trincaz-Duvoid,[16] B. Tuchming,[17] C. Tully,[64] A.S. Turcot,[68] P.M. Tuts,[65] L. Uvarov,[37] S. Uvarov,[37] S. Uzunyan,[49] B. Vachon,[5] R. Van Kooten,[51] W.M. van Leeuwen,[31] N. Varelas,[48] E.W. Varnes,[42] I.A. Vasilyev,[36] M. Vaupel,[25] P. Verdier,[15] L.S. Vertogradov,[33] M. Verzocchi,[57] F. Villeneuve-Seguier,[40] J.-R. Vlimant,[16] E. Von Toerne,[55] M. Vreeswijk,[31] T. Vu Anh,[15] H.D. Wahl,[46] R. Walker,[40] L. Wang,[57] Z.-M. Wang,[67] J. Warchol,[52] M. Warsinsky,[21] G. Watts,[76] M. Wayne,[52] M. Weber,[47] H. Weerts,[61] M. Wegner,[20] N. Wermes,[21] A. White,[72] V. White,[47] D. Whiteson,[43] D. Wicke,[47] D.A. Wijngaarden,[32] G.W. Wilson,[54] S.J. Wimpenny,[45] J. Wittlin,[58] M. Wobisch,[47] J. Womersley,[47] D.R. Wood,[59] T.R. Wyatt,[41] Q. Xu,[60] N. Xuan,[52] R. Yamada,[47] M. Yan,[57] T. Yasuda,[47] Y.A. Yatsunenko,[33] Y. Yen,[25] K. Yip,[68] S.W. Youn,[50] J. Yu,[72] A. Yurkewicz,[61] A. Zabi,[15] A. Zatserklyaniy,[49] M. Zdrazil,[67] C. Zeitnitz,[23] D. Zhang,[47] X. Zhang,[70] T. Zhao,[76] Z. Zhao,[60] B. Zhou,[60] J. Zhu,[57] M. Zielinski,[66] D. Zieminska,[51] A. Zieminski,[51] R. Zitoun,[67] V. Zutshi,[49] E.G. Zverev,[35] and A. Zylberstejn[17]
(DØ Collaboration)

[1] *Universidad de Buenos Aires, Buenos Aires, Argentina*
[2] *LAFEX, Centro Brasileiro de Pesquisas Físicas, Rio de Janeiro, Brazil*
[3] *Universidade do Estado do Rio de Janeiro, Rio de Janeiro, Brazil*
[4] *Instituto de Física Teórica, Universidade Estadual Paulista, São Paulo, Brazil*
[5] *Simon Fraser University, Burnaby, Canada, University of Alberta, Edmonton, Canada, McGill University, Montreal, Canada and York University, Toronto, Canada*
[6] *Institute of High Energy Physics, Beijing, People's Republic of China*
[7] *Universidad de los Andes, Bogotá, Colombia*
[8] *Charles University, Center for Particle Physics, Prague, Czech Republic*
[9] *Czech Technical University, Prague, Czech Republic*
[10] *Institute of Physics, Academy of Sciences, Center for Particle Physics, Prague, Czech Republic*
[11] *Universidad San Francisco de Quito, Quito, Ecuador*
[12] *Laboratoire de Physique Corpusculaire, IN2P3-CNRS, Université Blaise Pascal, Clermont-Ferrand, France*
[13] *Laboratoire de Physique Subatomique et de Cosmologie, IN2P3-CNRS, Universite de Grenoble 1, Grenoble, France*
[14] *CPPM, IN2P3-CNRS, Université de la Méditerranée, Marseille, France*
[15] *Laboratoire de l'Accélérateur Linéaire, IN2P3-CNRS, Orsay, France*
[16] *LPNHE, Universités Paris VI and VII, IN2P3-CNRS, Paris, France*
[17] *DAPNIA/Service de Physique des Particules, CEA, Saclay, France*
[18] *IReS, IN2P3-CNRS, Université Louis Pasteur, Strasbourg, France and Université de Haute Alsace, Mulhouse, France*
[19] *Institut de Physique Nucléaire de Lyon, IN2P3-CNRS, Université Claude Bernard, Villeurbanne, France*
[20] *RWTH Aachen, III. Physikalisches Institut A, Aachen, Germany*
[21] *Universität Bonn, Physikalisches Institut, Bonn, Germany*
[22] *Universität Freiburg, Physikalisches Institut, Freiburg, Germany*
[23] *Universität Mainz, Institut für Physik, Mainz, Germany*
[24] *Ludwig-Maximilians-Universität München, München, Germany*
[25] *Fachbereich Physik, University of Wuppertal, Wuppertal, Germany*
[26] *Panjab University, Chandigarh, India*
[27] *Tata Institute of Fundamental Research, Mumbai, India*
[28] *University College Dublin, Dublin, Ireland*
[29] *Korea Detector Laboratory, Korea University, Seoul, Korea*
[30] *CINVESTAV, Mexico City, Mexico*
[31] *FOM-Institute NIKHEF and University of Amsterdam/NIKHEF, Amsterdam, The Netherlands*
[32] *University of Nijmegen/NIKHEF, Nijmegen, The Netherlands*

[33] Joint Institute for Nuclear Research, Dubna, Russia
[34] Institute for Theoretical and Experimental Physics, Moscow, Russia
[35] Moscow State University, Moscow, Russia
[36] Institute for High Energy Physics, Protvino, Russia
[37] Petersburg Nuclear Physics Institute, St. Petersburg, Russia
[38] Lund University, Lund, Sweden, Royal Institute of Technology and Stockholm University, Stockholm, Sweden and Uppsala University, Uppsala, Sweden
[39] Lancaster University, Lancaster, United Kingdom
[40] Imperial College, London, United Kingdom
[41] University of Manchester, Manchester, United Kingdom
[42] University of Arizona, Tucson, Arizona 85721, USA
[43] Lawrence Berkeley National Laboratory and University of California, Berkeley, California 94720, USA
[44] California State University, Fresno, California 93740, USA
[45] University of California, Riverside, California 92521, USA
[46] Florida State University, Tallahassee, Florida 32306, USA
[47] Fermi National Accelerator Laboratory, Batavia, Illinois 60510, USA
[48] University of Illinois at Chicago, Chicago, Illinois 60607, USA
[49] Northern Illinois University, DeKalb, Illinois 60115, USA
[50] Northwestern University, Evanston, Illinois 60208, USA
[51] Indiana University, Bloomington, Indiana 47405, USA
[52] University of Notre Dame, Notre Dame, Indiana 46556, USA
[53] Iowa State University, Ames, Iowa 50011, USA
[54] University of Kansas, Lawrence, Kansas 66045, USA
[55] Kansas State University, Manhattan, Kansas 66506, USA
[56] Louisiana Tech University, Ruston, Louisiana 71272, USA
[57] University of Maryland, College Park, Maryland 20742, USA
[58] Boston University, Boston, Massachusetts 02215, USA
[59] Northeastern University, Boston, Massachusetts 02115, USA
[60] University of Michigan, Ann Arbor, Michigan 48109, USA
[61] Michigan State University, East Lansing, Michigan 48824, USA
[62] University of Mississippi, University, Mississippi 38677, USA
[63] University of Nebraska, Lincoln, Nebraska 68588, USA
[64] Princeton University, Princeton, New Jersey 08544, USA
[65] Columbia University, New York, New York 10027, USA
[66] University of Rochester, Rochester, New York 14627, USA
[67] State University of New York, Stony Brook, New York 11794, USA
[68] Brookhaven National Laboratory, Upton, New York 11973, USA
[69] Langston University, Langston, Oklahoma 73050, USA
[70] University of Oklahoma, Norman, Oklahoma 73019, USA
[71] Brown University, Providence, Rhode Island 02912, USA
[72] University of Texas, Arlington, Texas 76019, USA
[73] Southern Methodist University, Dallas, Texas 75275, USA
[74] Rice University, Houston, Texas 77005, USA
[75] University of Virginia, Charlottesville, Virginia 22901, USA
[76] University of Washington, Seattle, Washington 98195, USA

(Dated: October 25, 2004)

Using the data collected with the DØ detector at $\sqrt{s} = 1.96$ TeV, for integrated luminosities of about 180 pb^{-1}, we have measured the ratio of inclusive cross sections for $p\bar{p} \rightarrow Z + b$ jet to $p\bar{p} \rightarrow Z+$jet production. The inclusive $Z+b$-jet reaction is an important background to searches for the Higgs boson in associated ZH production at the Fermilab Tevatron collider. Our measurement is the first of its kind, and relies on the $Z \rightarrow e^+e^-$ and $Z \rightarrow \mu^+\mu^-$ modes. The combined measurement of the ratio yields 0.023 ± 0.005 for hadronic jets with transverse momenta $p_T > 20$ GeV/c and pseudorapidities $|\eta| < 2.5$, consistent with next-to-leading order predictions of the standard model.

PACS numbers: 14.70.Hp, 14.65.Fy

Inclusive $Z+b$-jet production is expected to be a major background to Higgs production in the $p\bar{p} \rightarrow ZH$ channel, with subsequent Higgs-boson decays into $b\bar{b}$. The parton-level subprocesses expected to contribute to the $Z + b$-jet final state are $bg \rightarrow Zb$ (where g stands for a gluon), and $q\bar{q} \rightarrow Zg$, with $g \rightarrow b\bar{b}$ [1]. The process $bg \rightarrow Zb$, where the initial b is from the sea of the proton parton distribution, is predicted to account for approximately two thirds of the total inclusive cross section $\sigma(p\bar{p} \rightarrow Z + b$ jet) at $\sqrt{s} = 1.96$ TeV. The b-quark density of the proton influences the production rates of single top quarks and the final state hb, with h representing a supersymmetric Higgs boson. Consequently, the measurement of $Z+b$ jet production is an important step in constraining the b-quark density of protons.

In this Letter, we describe a measurement of the ratio of production cross sections of inclusive $Z+b$ jets to Z+jets. The measurement of the ratio benefits from cancellations of many systematic uncertainties, such as the 6.5% uncertainty in the luminosity, and therefore allows a more precise comparison with theory.

We search for Z bosons in association with hadronic jets in about 180 pb^{-1} of data collected at the DØ experiment between August 2002 and September 2003. The DØ detector at the Fermilab Tevatron collider is a general-purpose detector comprising a magnetic central-tracking, preshower, calorimeter, and muon systems [2]. The central-tracking system consists of a silicon microstrip tracker (SMT) and a central fiber tracker, both located within a 2 T superconducting solenoidal magnet. The design was optimized for tracking and vertexing capabilities at pseudorapidities $|\eta| < 3$, where $\eta = -\ln(\tan(\theta/2))$ and θ is the polar angle with respect to the proton beam direction (z). Particle energies are measured in three liquid-argon/uranium calorimeters: A central calorimeter (CC) covers $|\eta| < 1.1$, and two end calorimeters (EC) extend coverage to $|\eta| < 4.2$, each calorimeter housed in a separate cryostat [3]. Central and forward preshower detectors are located just outside of the superconducting coil (in front of the calorimetry), and additional scintillators between the CC and EC cryostats provide sampling of developing showers for $1.1 < |\eta| < 1.4$. The muon detection system is outside the calorimetry and consists of a layer of tracking detectors and scintillation trigger counters before 1.8 T iron toroid magnets, followed by two similar layers after the toroids. The trigger and data acquisition systems are designed to accommodate high luminosities.

The dielectron sample is selected from the data by requiring two clusters of energy in the electromagnetic (EM) layers at the trigger level. In the offline selection, two EM clusters are each required to have transverse momentum $p_T > 15$ GeV/c and $|\eta| < 2.5$. In addition, the shower development in the calorimeter and isolation from hadronic activity must be consistent with that expected of an electron, and at least one of the EM clusters is required to have an associated track to maximize the possibility of having a Z boson in the event. The electron candidates with matching tracks are to required to have a ratio of measured energy in the calorimeter to momentum measured with the tracking system consistent with that expected of an electron. The Z candidates are selected by requiring a dielectron mass (m_{ee}) of 80 GeV/$c^2 < m_{ee} <$ 100 GeV/c^2. The Z+jet sample is then selected by requiring the presence of at least one reconstructed hadronic jet with $p_T > 20$ GeV/c and $|\eta| < 2.5$.

Jets are reconstructed from calorimeter clusters using a cone algorithm of cone size $\Delta\mathcal{R} = \sqrt{(\Delta\eta)^2 + (\Delta\phi)^2} = 0.5$ in pseudorapidity and azimuth(ϕ). Hadronic jets are required to have an associated cluster of tracks ("track jets"). This requirement reduces background from noise in the calorimeter. Track jets are found by applying a cone track clustering algorithm of size $\Delta\mathcal{R} = 0.5$ with a seed track of $p_T > 1.0$ GeV/c, to tracks of $p_T > 0.5$ GeV/c that are close to the primary interaction vertex (whose determination is discussed below). A track jet can consist of two or more tracks.

A "taggable" jet is a calorimeter jet with a matching track jet within $\Delta\mathcal{R} < 0.5$. Applying the taggability criterion to 2,661 jets in 2,219 $Z(ee)$ candidate events in the mass Z window yields 1,658 events. Based on side bands to the Z mass window, 121 ± 4 events are estimated to be from background sources. The main background is from multijet production where two jets mimic EM objects, with one of the objects having an overlapping track that passes the track-matching criteria. The taggability per jet is $(75 \pm 1)\%$ after background subtraction.

The dimuon sample is defined by the detection of at least one muon candidate at the trigger level. In the offline selection, two isolated muons are required to be of opposite charge, and to have $p_T > 15$ GeV/c and $|\eta| < 2$ with trajectories in the muon spectrometer matched to tracks in the central-tracking detector. Muon isolation is based on the transverse component of the muon momentum relative to the combined momenta of muon and the closest calorimeter jet in (η, ϕ) space, and is $p_{Trel} > 10$ GeV/c. The Z candidates are selected by requiring a dimuon mass of 65 GeV/$c^2 < m_{\mu\mu} <$ 115 GeV/c^2. The Z mass window is larger than in the dielectron channel due to worse momentum resolution for high p_T muons. The criteria for reconstructed hadronic jets are the same as in the dielectron channel. A total of 1,406 events remain after the requirement that there be at least one taggable jet. The main background in this channel is from $b\bar{b}$ production, where both b jets contain muons that satisfy the isolation criterion (referred to as $b\bar{b}$ background). The isolation efficiencies of muons from Z and $b\bar{b}$ are expected to be different, since, for the latter, a hadronic jet would be expected to be close to the muon. By performing fits to dimuon mass spectra, where the background contributes to the continuum, samples with different number of isolated muons are analyzed to measure the isolation efficiencies and background rates. From such analyses, we estimate that the background contribution to the final sample with two isolated muons is 17.5 ± 4.1 events.

Figure 1 shows distributions in transverse momentum of taggable jets for both channels (points with error bars), compared to a $Z+$jet Monte Carlo (MC) generated with ALPGEN [4], using PYTHIA [5] for parton showering and hadronization. Also shown is a background estimation based on data obtained from samples that are in the

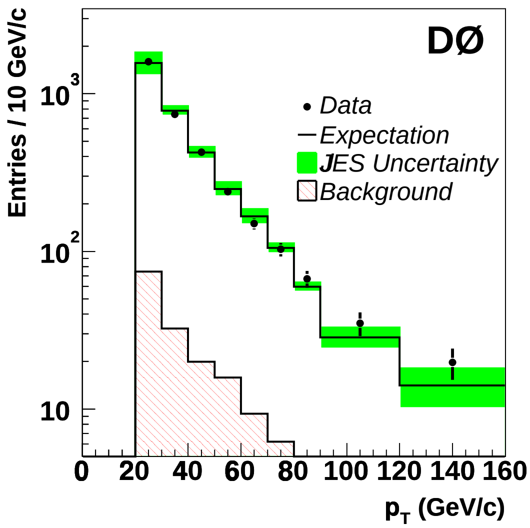

FIG. 1: The p_T distribution of taggable jets in dielectron and dimuon channels compared to Z+jet ALPGEN with PYTHIA showering and full detector simulation (open histogram), and background (multijet for ee channel and $b\bar{b}$ background for $\mu\mu$ channel) derived from data. The error bars on the data points are statistical. The prediction is normalized to the data, as described in the text.

side band for the dielectron channel, or fail the isolation criterion for the dimuon channel. The background distribution is normalized to the number of background events estimated in the selected sample. The simulated signal is then normalized so that the total agrees with the measurement in Fig. 1. Within the uncertainty of the jet energy scale (JES), indicated by the darker shading about the expectation, the shape of the distribution is well-described by the simulation.

The b quark fragments into a B hadron, which is identified by a displaced secondary vertex that is separated from the primary vertex. The reconstruction of secondary vertices proceeds in two steps. First, the primary interaction vertex is identified, and then additional nearby vertices are reconstructed. In the high luminosity environment of the Fermilab Tevatron collider, there can be more than one interaction per beam crossing, one of which is likely to have triggered the recorded event. The interaction region in DØ has a root mean-square width of $\approx$ 25 cm along z, with a transverse beam size of $\approx$ 30 μm. It is possible to distinguish the main hard-interaction vertex from any additional soft interactions because the vertices are normally well-separated along z. Primary interaction vertices are reconstructed in two passes. In the first pass, all tracks present in an event are used to find seed vertices using an iterative method, where tracks that contribute to a fit to a common vertex with a χ^2/d.o.f. greater than some chosen threshold are removed. The fit is repeated until a stable set of seeds is obtained. The seed vertices are then used in a second pass to fit all tracks within a certain distance-of-closest-approach to any seed. This improves the position resolution on the vertex, since the fit is less affected by poorly reconstructed tracks. The p_T distribution of the associated tracks is then used to select the primary interaction vertex (PV).

A b-jet tagging algorithm for secondary vertices (SV) is used to identify heavy-quark jets in the analysis. Tracks that are displaced from the PV in the transverse plane are used as seeds to find secondary vertices. First, a fixed-cone jet algorithm of $\Delta\mathcal{R} = 0.5$ is used to cluster the tracks to form track-jets. Tracks are required to have hits in at least two layers of the SMT, $p_T > 0.5$ GeV/c, and be within 0.15 cm in the plane transverse to z and 0.40 cm in z relative to the PV. Tracks identified as arising from K^0_S and Λ decays or photon conversions are not considered. Any pair of tracks within a track-jet with an impact parameter relative to the hard-interaction vertex (distance of closest approach – dca – of a track to a vertex in the plane transverse to the z direction) divided by their uncertainties (σ_{dca}), dca/$\sigma_{\mathrm{dca}} > 3$ is used as a seed for secondary vertices. Additional tracks are attached iteratively to the seed vertices if their χ^2-contribution to the vertex fit is consistent with originating from the vertex. A secondary vertex consists of two or more tracks. The momentum vector of the SV is defined as the vector sum of track momenta. Finally, good-quality secondary vertices are selected based on the decay length (distance between PV and SV), collinearity of the vertex momentum with the direction from PV to SV, and vertex-fit χ^2. A jet is considered b tagged when it is taggable and has at least one secondary vertex, with a decay-length transverse to the PV (L_{xy}) divided by its uncertainty $L_{xy}/\sigma_{xy} > 7$, associated with it. A secondary vertex is associated to a jet if the opening angle between the direction of the calorimeter-based jet axis and the momentum vector of the SV is $\Delta\mathcal{R} < 0.5$.

The b-tagging efficiency (ϵ_b) and the light-flavor tagging rate (ϵ_L) of the b-tagging algorithm are parametrized as functions of jet p_T and η. The parametrization of ϵ_b is derived from a different data sample using events with jets containing muons (muonic jets), which are dominated by b jets, but also have contributions from light quark jets, gluon jets, and charm jets. The b-tagging efficiency is extracted from the heavy-flavor component in this muonic jet sample. The light-flavor tagging rate is also derived from data, after compensating for effects of displaced vertices that do not originate from heavy-flavor decay (K^0_S, Λ, and photon conversions). Different types of samples are used to determine ϵ_L and ϵ_b, and the spreads are taken as systematic uncertainties.

A comparison of inclusive Z+jet events, generated with the ALPGEN leading-order matrix element and PYTHIA for showering, with inclusive $Z + b$ events generated with PYTHIA, shows good agreement for jet p_T and η distributions. We therefore use the shapes of p_T and

η derived from the Z+jet data sample to estimate the expected b-tagging efficiency and the light-flavor tagging ("mistag") rate. The average b-tagging efficiency and mistag rate per jet, averaged over p_T and η, are found to be $(32.8 \pm 1.3)\%$ and $(0.25 \pm 0.02)\%$, respectively, for the dielectron channel. Corresponding values for the dimuon channel are $(33.1 \pm 1.1)\%$ and $(0.24 \pm 0.02)\%$. To obtain the event mistag rate, we take into consideration jet multiplicity, and measure the event mistag rate of 0.28% (0.27%) for the dielectron (dimuon) channel.

Since ϵ_b is derived from events with a muon embedded in a jet, whereas most of the b-tagged jets do not contain such muons, the difference in b-tagging efficiencies for hadronic b jets and muonic b jets is derived from MC, and the ratio is used to correct ϵ_b. We cannot at this point derive the charm tagging efficiency (ϵ_c) from data, so we rely on PYTHIA MC to compare $Z \to b\bar{b}$ and $Z \to c\bar{c}$ samples. We assume that $(\epsilon_c/\epsilon_b)_{\rm data} = (\epsilon_c/\epsilon_b)_{\rm MC} = 0.266 \pm 0.003$.

The jet taggability, t_L, is measured using data to be $(75 \pm 1)\%$, while that for b jets, t_b, is obtained from MC, and scaled such that $(t_b)_{\rm data} = (t_L)_{\rm data} \times (\frac{t_b}{t_L})_{\rm MC}$. The result is $(t_b)_{data} = (79.2 \pm 1.3)\%$ for the dielectron channel and $(80.7 \pm 1.1)\%$ for the dimuon channel. We assume that the taggability of charm jets is same as t_b.

After applying b tagging, 27 $Z(\to ee)+b$-jet candidate events are left, with an expected background from the Drell-Yan ee continuum and multijet background of 4.2 ± 1.4 events based on the side-band subtraction method. In the dimuon channel, 22 events are observed with 5.0 ± 1.1 events from $b\bar{b}$ background.

After subtracting the background contributions, two equations, one before and the other after the requirement of b tagging, determine the contributions from different flavors in the remaining events:

$$N_{\rm before\ b-tag} = t_b N_b + t_c N_c + t_L N_L \quad (1)$$
$$N_{\rm b-tagged} = \bar{\epsilon}_b t_b N_b + \bar{\epsilon}_c t_c N_c + \bar{\epsilon}_L t_L N_L, \quad (2)$$

where N_b, N_c and N_L are the numbers of events with b, c and light jets, respectively; t_i are the taggabilities per event for different jet types; and the $\bar{\epsilon}_i$ are the corresponding mean event-tagging efficiencies. We assume that the tagging efficiencies per jet, $\bar{\epsilon}_b$ and $\bar{\epsilon}_c$, are the same as the tagging efficiencies per event. Equations (1) and (2) have three unknowns. We take the theoretical prediction of $N_c = 1.69 N_b$ [1], to provide a solution of Eqs. (1) and (2) for N_b, N_c and N_L.

The ratio $\sigma(p\bar{p} \to Z + b\ \text{jet})/\sigma(p\bar{p} \to Z\text{+jet}) = N_b/(N_b + N_c + N_L)$ is found to be 0.026 ± 0.007 for the dielectron channel and 0.020 ± 0.005 for the dimuon channel, where the errors are purely statistical. The combined ratio, using the statistical weighting of the number of observed Z+jet candidates, is 0.023 ± 0.004. The shape of the p_T spectrum for b-tagged jets and the significance of decay lengths of secondary vertices are compared to the

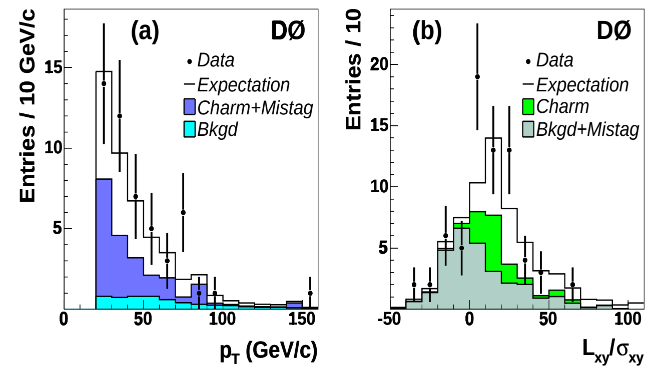

FIG. 2: (a) The p_T spectrum for b-tagged jets. (b) Distribution in decay-length significance of secondary vertices in the transverse plane, without the requirement on decay-length significance. All error bars are statistical.

TABLE I: Systematic uncertainties for the combined ratio of cross sections, showing the impact of ± 1 standard deviation changes in contributions.

Source	Upward (%)	Downward (%)
Jet energy scale	5.7	6.7
Background estimate	5.6	5.3
$Z + (Q\bar{Q})$	0.0	5.5
Mistag rate	3.5	3.3
b/c tagging efficiency	3.1	3.2
Taggability	1.9	3.7
Correction for hadronic jet	2.0	1.7
Jet reconstruction efficiency	1.8	1.8
$\sigma(Z + c)/\sigma(Z + b)$	2.8	2.9
Total (added in quadrature)	10.2	12.3

sum of background and $Z + b$ MC in Fig. 2. The contribution of each component is given by the solution to Eqs. (1) and (2). The distribution of the decay-length significance for secondary vertices shows clear evidence for a heavy-flavor component in the b-tagged candidate events.

Sources of systematic uncertainty in the ratio include:

i) Jet energy scale. The JES is varied within its uncertainty. The JES for hadronic b jets is assumed to be the same as that for light-flavored jets, whereas in MC some differences are observed, and this effect is included as part of the JES uncertainty.

ii) Different methods of estimating background. The background is varied by its measured uncertainty and the ratio is recalculated.

iii) Jets that contain a $b\bar{b}$ or $c\bar{c}$ pair from gluon splitting. These jets have a higher tagging probability. The expected contribution is taken from theory [1], and the relative increase in $b(c)$-tagging efficiency is estimated from MC. This is labeled as $Z + (Q\bar{Q})$ in Table I.

iv) Mistag rate for light jets, which depends on the type of jet sample. Using events collected from hadronic jet triggers, the light-jet tagging efficiency is measured to be 0.23%, and for a sample of events with an enhanced EM fraction and small imbalance in overall p_T, this is 0.26%. A tagging efficiency of 0.25% per jet (or 0.28% per event) is obtained for the combined data.

v) Uncertainty in tagging efficiency for b and c jets is obtained by varying the efficiency by a ± 1 standard deviation, assuming complete correlation in the ratio of extracted cross sections. Also, for c jets, there is additional uncertainty from the ϵ_c/ϵ_b ratio obtained from MC. $\bar{\epsilon}_L$ is varied, as above, to estimate this effect.

vi) A small difference observed in t_b/t_L for different MC samples of $Z+b$ jet/Z+light jet, and $Z \to b\bar{b}/Z \to q\bar{q}$ is taken into account.

vii) Differences in tagging efficiency between hadronic jets and those containing muons. The b-tagging efficiency is measured in data using muonic jets. The tagging efficiency for hadronic jets is estimated to be 86% of that of muonic jets, as derived from $Z \to b\bar{b}$ MC. The same ratio in $Z + b\bar{b}$ MC is measured to be 84%, and the difference of 2% is taken as a systematic uncertainty.

viii) Different p_T-dependence in jet reconstruction for light, b, and c jets, measured using MC samples, is accounted for as a systematic uncertainty.

ix) Uncertainty from theory for the ratio $\sigma(Z + c\ \text{jet})/\sigma(Z + b\ \text{jet}) = N_c/N_b$ is estimated as 9.5% [1].

The effects of systematic uncertainties on the combined measurement are listed in Table I. All these uncertainties are assumed to be completely correlated for the two channels, except for that due to background estimation. Folding these uncertainties together, yields a ratio of $0.023 \pm 0.004(\text{stat})^{+0.002}_{-0.003}(\text{syst})$. This measurement is in good agreement with the next-to-leading order (NLO) prediction of 0.018 ± 0.004 [6].

In summary, we have presented the first inclusive measurement of b-jet production in association with Z bosons at the Fermilab Tevatron collider, which is a background to the standard-model Higgs searches in the ZH production channel. The measurement is in agreement with the NLO calculations and can be used to constrain the b-quark density of proton.

We thank the staffs at Fermilab and collaborating institutions, and acknowledge support from the Department of Energy and National Science Foundation (USA), Commissariat à l'Energie Atomique and CNRS/Institut National de Physique Nucléaire et de Physique des Particules (France), Ministry of Education and Science, Agency for Atomic Energy and RF President Grants Program (Russia), CAPES, CNPq, FAPERJ, FAPESP and FUNDUNESP (Brazil), Departments of Atomic Energy and Science and Technology (India), Colciencias (Colombia), CONACyT (Mexico), KRF (Korea), CONICET and UBACyT (Argentina), The Foundation for Fundamental Research on Matter (The Netherlands), PPARC (United Kingdom), Ministry of Education (Czech Republic), Natural Sciences and Engineering Research Council and WestGrid Project (Canada), BMBF and DFG (Germany), A.P. Sloan Foundation, Research Corporation, Texas Advanced Research Program, and the Alexander von Humboldt Foundation.

---

[*] Visitor from University of Zurich, Zurich, Switzerland.
[†] Visitor from Institute of Nuclear Physics, Krakow, Poland.

[1] J.M. Campbell, R.K. Ellis, F. Maltoni and S. Willenbrock, Phys. Rev. D **69**, 074021 (2004).
[2] V. Abazov *et al.*, in preparation for submission to Nucl. Instrum. Methods Phys. Res. A, and T. LeCompte and H.T. Diehl, "The CDF and DØ Upgrades for Run II", Ann. Rev. Nucl. Part. Sci. **50**, 71 (2000).
[3] S. Abachi *et al.*, Nucl. Instrum. Methods Phys. Res. A **338**, 185 (1994).
[4] M.L. Mangano, M. Moretti, F. Piccinini, R. Pittau and A. Polosa, J. High Energy Phys. **07**, 001 (2003).
[5] T. Sjöstrand *et al.*, Comput. Phys. Commun. **135**, 238 (2001).
[6] J.M. Campbell and S. Willenbrock (private communications).